High Power Density Design of Single-Phase AC/DC Converter with Active Power Decoupling Capability Utilizing Triangular Current Mode for LED Driver Applications

Hiroki Watanabe[1*] and Jun-ichi Itoh[1]
1 Department of Electrical, Electronics and Information Engineering,
Nagaoka University of Technology, Niigata, Japan
*E-mail: hwatanabe@vos.nagaokaut.ac.jp

***Abstract*— This paper proposes the Triangular Current Mode (TCM) control with the feedback control in order to compensate the current error due to the switching timing delay and the single-phase power ripple. In single-phase AC converter applications, it is well known that the double-line frequency power ripple increases the volume of the DC-link capacitor. On the other hand, TCM is the most simple and effective method to achieve ZVS for many converters. However, average current error occurs in TCM due to the switching timing delay. This paper proposes the TCM control with the feedback control in order to achieve the both of the active power decoupling control and the average current error compensation. The proposed TCM control compensates the current error between the average current command and the actual current by the feedback control. Furthermore, the second-order harmonics due to the power ripple is also compensated without the additional components. From the simulation result, it was confirmed that the current error of 23.0% was compensated by the proposed control. In addition, the second-order harmonics was reduced by 96.7%. Finally, the validity of the proposed control was confirmed by the experiment. As the experimental result, the current error of the DC component in the load current was reduced to 2.5% from 35%. Finally, the second-order harmonics was reduced by 86.7% by the proposed control.**

Keywords*— *AC/DC converter, Power decoupling, Triangular current mode, LED

I. INTRODUCTION

LED lighting markets have rapidly grown owing to the attractive advantage of their long life-time, low power consumption, and high luminance [1]-[3]. The LED driver requires the current source by the single-phase AC/DC converter which consists of the PFC converter and the DC/DC converter for dimming capability [4]-[6]. However, passive components such as the inductor and the capacitor may increases the circuit volume of the LED driver. Especially, an electrolytic capacitor is placed in LED drivers as the energy buffer to compensate the double-line frequency power ripple. However, the electrolytic capacitor may limit the life-time of LED driver systems [7].

The electrolytic capacitor-less AC/DC LED driver has been considered in order to solve this problem [8]. In ref. of [7], the Discontinuous Current Mode (DCM) is applied to remove the electrolytic capacitor from the LED driver circuit. However, highly peak current in DCM increses the conduction loss of the power converter.

Active power decoupling techniques are also commonly solution to remove the bulky electrolytic capacitor in single-phase AC applications [9]-[12]. This method adds the additional power decoupling circuit with the small decoupling capacitor to compensate the double-line frequency power ripple. In this method, a firm or ceramic capacitor is employed instead of the electrolytic capacitor for the energy storage of the power decoupling. However, the additional circuit may become a cause of decreasing conversion efficiency and power density of the LED driver circuit. Therefore, the reduction of the additional component is the important to improve these performances.

The Triangular Current Mode (TCM) is the simple way to improve the conversion efficiency [6]. This current mode has the triangular inductor current with the short negative current period. The attractive advantage of the current mode is that the Zero Voltage Switching (ZVS) is achieved without additional circuit and complicate control. Therefore, switching losses is drastically reduced compared to the other current mode of CCM and DCM.

TCM is implemented based on the Boundary Current Mode (BCM) control. In this case, the accurate switching control is necessary in order to obtain the targeted average inductor current because TCM is directly control the ripple current. However, the switching delay occurs due to some reason such as the dead-time, and signal delay of the gate driver, zero current detection. In LED applications, the accurate average current control is important for the dimming of LEDs.

This paper proposes the active power decoupling control with the improved TCM control. The originality of this paper is that the proposed TCM includes the feedback control in order to compensate the error current between the average current command and the actual current. As the result, the accurate average current control is possible

by the proposed TCM control. In addition, the proposed control has the capability of the active power decoupling because the double-line frequency component in the DC current is also compensated by the proposed feedback control. Therefore, the proposed control provides the ZVS operation and the active power decoupling capability without additional components to improve the power density and the conversion efficiency.

In this paper, the circuit configuration and the detail of the proposed control is presented.

II. Circuit Configuration

Fig.1 shows the conventional circuit with the Power Factor Correction (PFC) converter. The conventional circuit consists of the diode bridge, the PFC converter, and the buck converter. According to fig.1, the DC-link capacitor of C_{dc} is necessary. Especially, C_{dc} requires the large capacitance because the double-line frequency power ripple should be compensated by C_{dc} to obtain the constant DC output power for LEDs. Therefore, the electrolytic capacitor is usually implemented in DC-link.

Fig.2 shows the proposed circuit which consists of the AC/DC converter and the power decoupling circuit. The PEM rectifier has the PFC capability in order to obtain the unity power factor. The power decoupling circuit consists based on the typical buck converter and the small power decoupling capacitor of C_{buf}. The power decoupling circuit compensates the double-line frequency power ripple without the bulky electrolytic capacitor in the DC-link.

The proposed circuit has the three inductors. However, the inductance of these inductor is designed to small because it is easy to increase the switching frequency owing the TCM with the ZVS operation.

Fig.3 shows the relationship between the DC output power, the single-phase AC power, and the buffer power of the decoupling capacitor [13]. In single-phase AC applications, the AC power is fluctuated by the twice of the grid frequency. Firstly, the instantaneous AC input power p_{in} is expressed as

$$p_{in} = \frac{V_{acp} I_{acp}}{2}(1-\cos 2\omega t) \quad (1)$$

where V_{acp} is the AC peak voltage, I_{acp} is the AC peak current, ω is the grid angular frequency. According to (1), the power ripple that contains double-line frequency of the AC output power appears at DC side. Therefore, the instantaneous power of P_{buf} should be controlled by

$$p_{buf} = \frac{1}{2} V_{acp} I_{acp} \cos 2\omega t \quad (2)$$

where the polarity of p_{buf} is defined as the positive when the buffer capacitor C_{buf} discharges. Owing to the active power decoupling, the load power becomes constant, and it is expressed as

$$p_{in} = \frac{1}{2} V_{acp} I_{acp} = V_{load} I_{load} \quad (3).$$

Fig.4 shows the relationship between the ripple voltage of buffer capacitor and the capacitance of C_{buf}. The buffer power in the C_{buf} is represented by

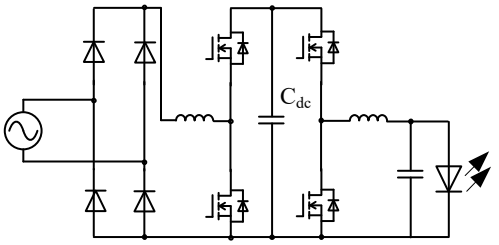

Fig.1. Conventional circuit with PFC converter. Electrolytic capacitor is placed in DC-link to compensate power ripple with double-line frequency.

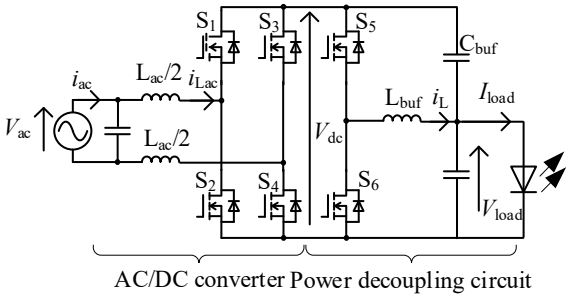

Fig.2. Proposed converter with active power decoupling circuit. Small energy buffer of C_{buf} compensates the double-line frequency power ripple instead of electrolytic capacitor.

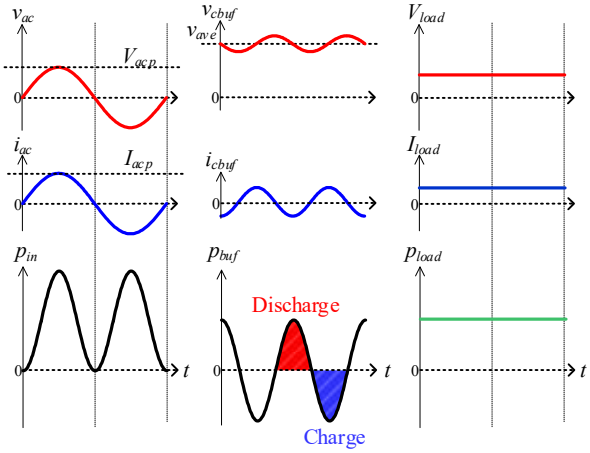

Fig.3. Relationship between DC input power, AC output power, and buffer power of energy storage.

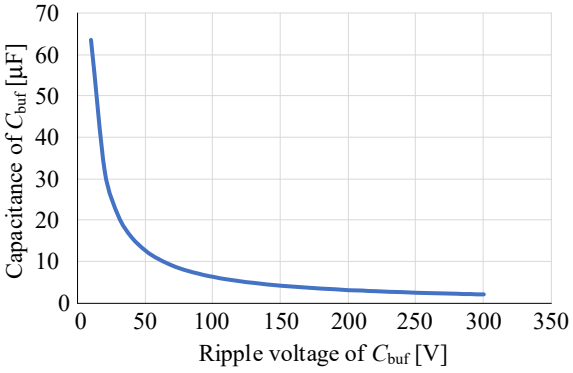

Fig.4. Relationship between buffer capacitor ripple voltage and capacitance of C_{buf}. The requirement of the capacitance for power decoupling decreases when large ripple voltage is allowed.

$$p_{cbuf} = \frac{1}{2}\omega C_{buf}\left\{\left(V_{ave} + \Delta\frac{V_{ripple}}{2}\right)^2 - \left(V_{ave} - \Delta\frac{V_{ripple}}{2}\right)^2\right\} \quad (4)$$

where P_{cbuf} is the buffer power of C_{buf}, ω is the grid angular frequency, V_{ave} is the average capacitor voltage, and V_{ripple} is the ripple voltage. The capacitance for the power decoupling is calculated from (4), and it is represented by

$$C_{buf} = \frac{P_{cbuf}}{\omega V_{ave}\Delta V_{ripple}} \quad (5).$$

According to fig.4, the capacitance for the power decoupling becomes small when the ripple voltage increases. The active power decoupling circuit swings the buffer capacitor voltage to reduce the capacitance of C_{buf}.

III. Control Method of Proposed Converter

A. Triangular current mode

Fig.5 shows the inductor current waveform in TCM and switching state of each switching devices. In the proposed circuit, TCM is implemented in both of the active power decoupling circuit and the AC/DC converter. The current mode of the power converter is classified into four modes of 1) Continuous Current Mode (CCM), 2) Discontinuous Current Mode (DCM), 3) Boundary Current Mode (BCM), and 4) TCM. TCM is the most simple and effective method to achieve ZVS. In TCM, the turn-on switching losses are reduced by ZVS, whereas the turn-off losses are greatly reduced by connecting a snubber capacitor in parallel with the switching devices. In TCM, the inductor current has the negative current period of T_{neg}. In the dead-time after T_{neg}, the parasitic capacitor of the switching devices is fully discharged owing to the negative current. As the result, ZVS is achieved when switch is turned-on as shown in fig.5.

TCM control requires the accurate switching control because this control does not refer the average current. However, the actual switching timing has delay due to the gate driver, the zero current detection circuit, and the switching characteristics of the switching devices. As the result, the average inductor current has the error from the targeted average current. In order to solve this problem, the current feedback control is added for TCM control. The detail of the proposed control is shown in next chapter.

B. Control block diagram of active power decoupling circuit

Fig.6 shows the control block diagram of the power decoupling circuit. TCM control is realized based on BCM control. Both of TCM and BCM control calculate the on-state period command in order to decide the average inductor current. Firstly, the on-state period in BCM is expressed as

$$T_{on\_BCM} = \frac{2L_{dc}}{V_{dc\_det} - V_{load\_det}} I_{ave}^{*} \quad (6)$$

where $T_{\mathrm{on\_BCM}}$ is the on-state period in BCM, L_{dc} is the boost inductor, and $V_{\mathrm{dc\_det}}$ is the detection value of DC input voltage of the power decoupling circuit, I_{ave}^{*} is the average current command for I_{load} of the load current. Ideally, the average current command and the load current should be matched. Actually, these current does not match

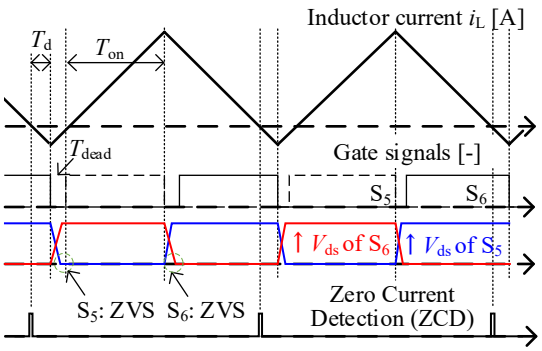

Fig.5. Inductor current and each switching waveforms of power decoupling circuit. ZVS is achieved by negative current when each switching devices are turned-on.

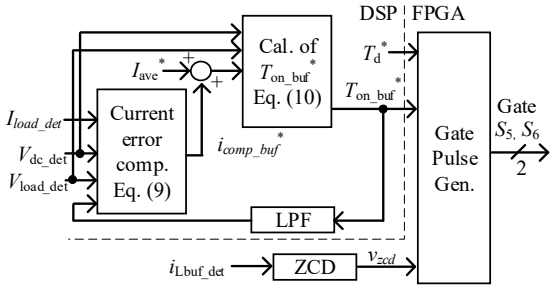

Fig.6. Control block diagram of active power decoupling circuit. TCM control is implemented in order to achieve ZVS.

due to the parameter mismatch and the switching delay, and the power ripple. Especially, the double-line frequency power ripple fluctuates the load current when the power decoupling is not applied. In particular, the dead time and the negative current in TCM are also become a cause of the current error because Eq. (4) does not consider the dead time and the negative current. Therefore, the feedback control is added in order to solve this problem. Relationship between the current command, the actual current, and the error current is expressed as

$$I_{ave}^{*} = I_{load} + I_{error} \quad (7)$$

$$T_{on\_buf} = \frac{2L_{dc}}{V_{dc} - V_{load}}\left(I_{load} + I_{error}\right) \quad (8)$$

where $T_{\mathrm{on\_buf}}$ is the on-state period, I_{error} is the error current between I_{ave}^{*} and I_{load}. Note that I_{error} becomes zero when I_{load} is match to I_{ave}^{*}. According to (8), the compensation current of $I_{\mathrm{comp\_buf}}^{*}$ is expressed as

$$I_{comp\_buf}^{*} = \frac{T_{on\_buf}^{*}(V_{dc\_det} - V_{load\_det})}{2L_{dc}} - I_{load\_det} \quad (9)$$

where $I_{\mathrm{dc\_det}}$ is the detection value of the DC input current of the power decoupling circuit. Finally, the on-state period command $T_{\mathrm{on\_buf}}^{*}$ in the proposed TCM is represented by

$$T_{on\_buf}^{*} = \frac{2L_{dc}}{V_{dc\_det} - V_{load\_det}}\left(I_{ave}^{*} + I_{comp\_buf}^{*}\right) \quad (10).$$

Owing to the current error compensator, the double-line frequency component in I_{load} is compensated, which means that the active power decoupling is achieved by the

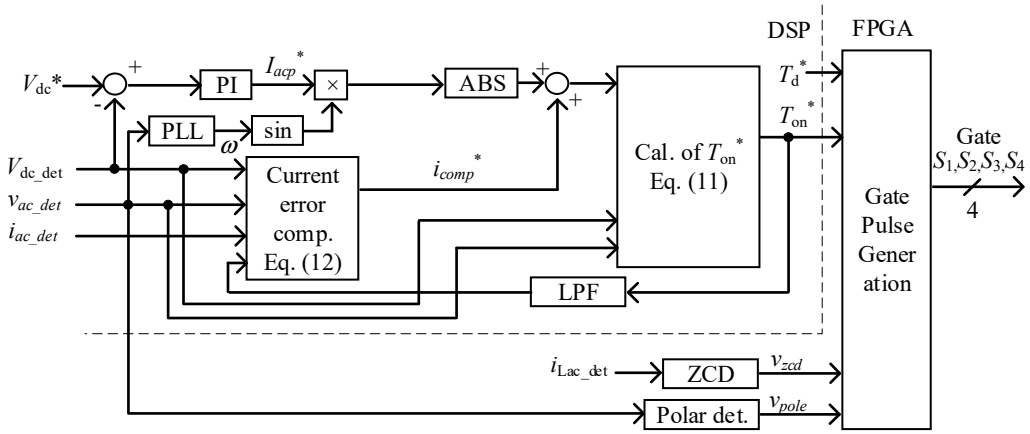

Fig.7. Control block diagram of AC/DC converter. TCM control is implemented in order to achieve ZVS. In particular, DC-link voltage control is added in AC/DC converter control.

proposed control. Note that T_{on}^* is necessary to calculate $I_{comp\_buf}^*$. Therefore, the low-pass filter with high cut-off frequency is added on the feedback pass of T_{on}^* in order to avoid the recursive calculation.

C. Control block diagram of AC/DC converter

Fig.7 shows the control block diagram of the AC/DC converter. The AC/DC converter control also applies the TCM control. The control method of the AC/DC converter is similar to the control of the power decoupling circuit. The on-state period of T_{on}^* is calculated by

$$T_{on}^* = \frac{2L_{ac}}{V_{dc\_det} + |v_{ac\_det}|}\left(\left|I_{acp}^* \sin \omega t\right| + i_{comp}^*\right) \quad (11)$$

where I_{acp}^* is the amplitude command of the AC input current. The AC/DC converter control also applies the DC voltage control in order to regulate the DC-link voltage more that the peak grid voltage. The DC-link voltage is controlled by the PI controller. In addition, the Phase Looked Loop (PLL) is applied in order to generate the current command in synchronized with the phase of the grid voltage.

The current error compensation of average inductor current for i_{ac} is also applied because the negative current increases the THD of the input current. The compensation current of I_{comp}^* is calculated same as $I_{comp\_buf}^*$ in the control of the active power decoupling circuit. I_{comp}^* is defined as

$$I_{comp}^* = \frac{T_{on}^*(V_{dc\_det} + |v_{ac\_det}|)}{2L_{ac}} - |i_{ac\_det}| \quad (12)$$

where i_{ac_det} is the detection value of the input current.

The AC/DC converter makes the sinusoidal AC input current. Note that the on-state command is defined as the positive value. Therefore, the switching state is changed based on the polarity of the grid voltage.

Fig.8 shows the switching state of the AC/DC converter. Each gate signals for the AC/DC converter is calculated by the absolute value. Therefore, the switching state of each switching devices is changed based on the grid voltage polar in order to provide the AC output current synchronized with the grid voltage as shown in fig.8.

Fig.8 shows the relationship between the bottom

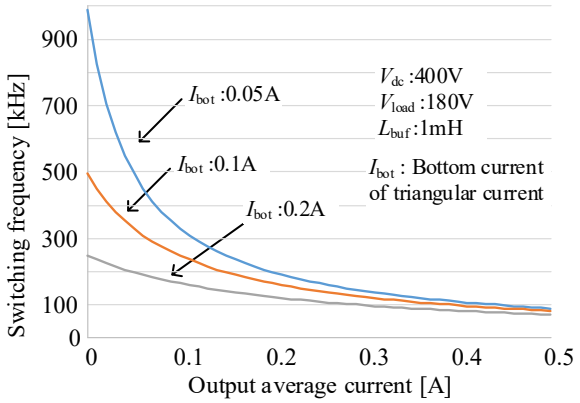

Fig.8. Relationship between Output average current and

current I_{dc} and the switching frequency in TCM. The switching frequency of TCM decreases when the input current increases, and it is calculated by

$$f_{sw} = \frac{1}{2L_{dc}(I_{bot} + I_{ave})\left(\frac{1}{V_{dc} - V_{load}} + \frac{1}{V_{load}}\right)} \quad (13)$$

where I_{bot} is the bottom current of the inductor current, V_{dc} is the DC-link voltage. According to fig.10, the switching frequency is decreased when I_{bot} is set to large because the negative di/dt period in the inductor current increases to make the large bottom current. Therefore, the bottom current in TCM influences to the ZVS characteristics and the switching frequency design.

IV. SIMULATION RESULT

Table I shows the simulation parameter. Fig.9 (a) shows the simulation result without proposed feedback control. Note that the led line means that the low pass filter with 10kHz of the cutoff frequency is added to confirm the fundamental waveforms. According to fig. 9 (a), the average DC-link voltage is match to the command value

of the voltage control. In addition, the sinusoidal grid current waveform is obtained by the TCM control. However, the average load current becomes low compared to the command value due to the bottom current. In particular, the load current is fluctuated by the power ripple with double-line frequency.

Fig. 9 (b) shows the simulation result with proposed feedback control. According to fig. 9 (b), the load current without the double-line frequency component is obtained owing to the proposed control. Especially, the average current is matched to the command value. On the other hand, the inductor current is fluctuated at the double-line frequency because the buffer capacitor is charged and discharged for the power decoupling. As the result, the ripple voltage in the DC-link voltage becomes large compared to without the proposed control. In particular, the sinusoidal grid current waveform was also obtained same as fig. 10 (a). According to fig. 9, the validity of the proposed control was confirmed.

Fig.10 shows the harmonic analysis result of the load current. Note that the blue line means the without proposed control, the red line means the with proposed control. According to fig. 10, the load current without proposed method has 27.3% of the current error. On the other hand, this current error was completely compensated by the proposed control. As the result, the DC component with the proposed control is match to the command value. In particular, the second-order harmonics in the load current is reduced by 96.3% owing to the proposed control.

V. Experimental Result

The proposed control was tested by the prototype circuit with rated power of 40 W. Table. II shows the experimental parameters. According to table II, The Input voltage is $100V_{rms}$, the decoupling capacitor is 13μF, the average current command for the load current is set to 0.4A. In addition, 2.5μsec of the turn-on delay is added in order to generate the negative current in each inductor current for TCM.

Fig. 11 shows the experimental result. According to fig. 11 (a), the average current of the load current does not match to the current command of 0.4A because the current command is calculated by the boundary current mode condition as shown in (6) although actual current mode is TCM. Actually, it can adjust by considering the negative current period. However, the inaccuracy switching due to the delay of the gate driver, zero current detection also become a cause of the negative current. Actually, it is difficult to adjust the negative current due to these delays. Moreover, the load current has the second-order harmonics component due to the single-phase power ripple with the double-line frequency owing to small decoupling capacitor.

Fig. 11 (b) shows the experimental result with the proposed control. According to fig. 11 (b), it was confirmed that the average load current is also matched to the average current command of 0.4A. In addition, the second-order harmonics in the load current was removed by the proposed control. Moreover, the sinusoidal input AC current with high power factor was obtained by the AC/DC converter.

Fig. 12 shows the inductor current of the AC/DC converter and the power decoupling circuit. According to fig.12, it was confirmed that the negative current for TCM was obtained both converters.

Table I. Simulation parameter

Symbol	Quantity	Value
V_{ac}	Input voltage	200 Vrms
P_{in}	Input power	40 W
L_{buf}	Inductor	500 μH
L_{ac}	Grid-tied Inductor	500 μH
C_{buf}	Decoupling capacitor	15 μF
I_{ave}^*	Average current command	0.22 A
V_{dc}^*	DC-link voltage command	400 V

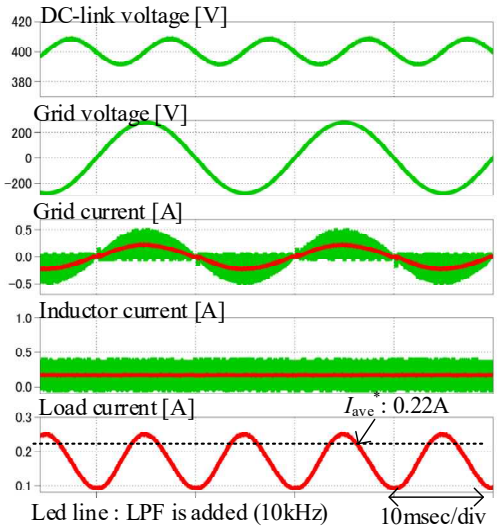

(a) Without proposed control

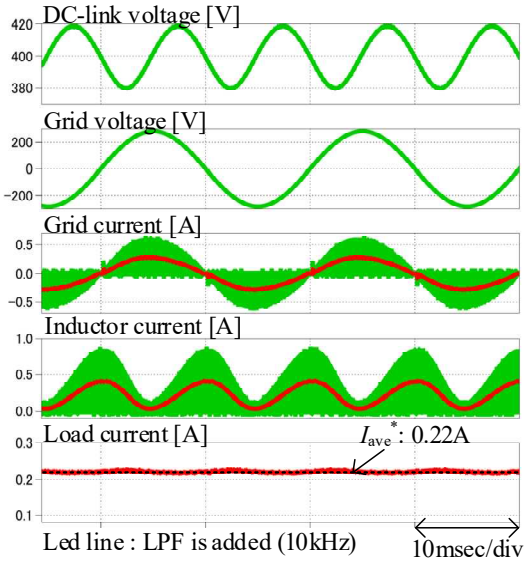

(b) With proposed control

Fig.9 Simulation result.

Fig. 13 shows the harmonic analysis result of the load current. According to fig. 13, the DC component has the error of 35% when the proposed control is not applied. In addition, the load current has the second-order harmonics due to the single-phase power ripple. On the other hand, the current error in DC component became 2.5% when the proposed control is applied. Finally, the second-order harmonics was reduced by 86.7% owing to the proposed control.

VI. CONCLUSION

This paper proposed TCM control with the feedback control. TCM achieves the ZVS operation in order to reduce the switching losses. However, the load current is fluctuated at the double-line frequency due to the power ripple when the conventional TCM control is applied. The proposed TCM control achieves the compensation of the double-line frequency power ripple by the feedback control. In addition, the proposed TCM control compensates the current error between the average current command and the actual current. From the simulation results, it was confirmed that the current error of 23% was compensated by the proposed control. In addition, the second-order harmonics was reduced by 96.7%. Finally, the validity of the proposed control was confirmed by the experiment. As the experimental result, the current error of the DC component in the load current was reduced to 2.5% from 35%. Finally, the second-order harmonics was reduced by 86.7% by the proposed control.

REFERENCES

[1] H. Broeck, G. Sauerlander, and M. Vendt, "Power driver topologies and control schemes for LEDs," *IEEE Applied Power Electronics Conference and Exposition (APEC)*, pp. 1319–1325, (2007).

[2] M. S. Shur and A. Zukauskas, "Solid-state lighting: Toward superior illumination", *Proceedings of IEEE*, Vol. 93, No. 10, pp. 1691– 1703, (2005).

[3] Z. Shan, X. Chen,S. Fan,J. Jatskevich,C. K. Tse "An Electrolytic Capacitor-Less AC-DC LED Driver with a Low Power Processing Auxiliary Circuit and Ceramic Capacitors for Ripple Power Decoupling", *IEEE Energy Conversion Congress and Exposition (ECCE)*, pp. 5101–5108, (2018)

[4] R. Dayal, K. Modepalli, L. Parsa "A direct AC LED driver with high power factor without the use of passive components," *IEEE Energy Conversion Congress and Exposition (ECCE)*, pp. 4230–4234, (2012)

[5] H. Yamanaka, H. Yamada, "Dual Active Bridge DC-DC Converter based Wide Dimming Range LED Driver With High Speed Turn-Off for High-Brightness LED Floodlight" *IEEE Jour. of Ind. App.*, vol. 8, no.3, pp. 556–557, (2019)

[6] K. Yamamoto, R. Lum, H. Takahashi, "A Completely Capacitor-less, LED-switching Offline Lighting System" *IEEE Jour. of Ind. App.*, vol. 8, no.2, pp. 379–385, (2019)

[7] J. He, X. Ruan, L. Zhang, "Adaptive Voltage Control for Bidirectional Converter in Flicker-Free Electrolytic Capacitor-Less AC-DC LED Driver" *IEEE Trans. on Ind. Electron.*, vol. 64, no.1, pp. 320–324, (2016)

[8] B. Wang, X. Ruan, K.Yao, and M.Xu "A Method of Reducing the Peak-to-Average Ratio of LED Current for Electrolytic Capacitor-Less AC–DC Drivers," *IEEE Trans. on Power Electron.*, vol. 25, no.3, pp. 592–601, (2010)

[9] C. S. Wong, K. H. Loo, Y. M. Lai, C. K. Tse "Current-source PFC based LED drivers with electronic-smoothing inductor for AC power decoupling", *2017 19th European Conference on*

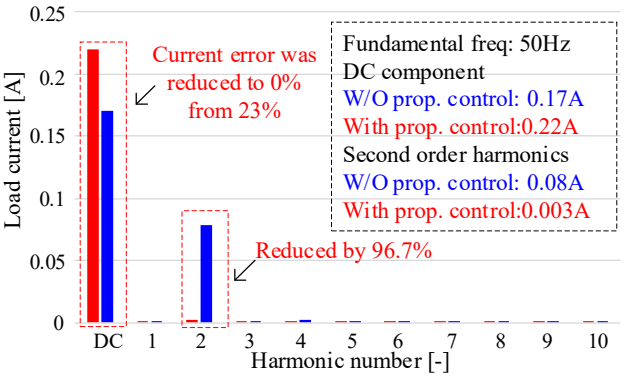

Fig.10 Harmonic analysis result of load current.

Table II. Experimental parameter

Symbol	Quantity	Value
V_{ac}	Grid voltage	100 V_{rms}
f_{ac}	Grid frequency	50 Hz
L_{buf}	Inductor	2 mH
L_{ac}	Grid-tied Inductor	2 mH
C_{buf}	Decoupling capacitor	13 μF
I_{ave}^*	Average current command	0.4 A

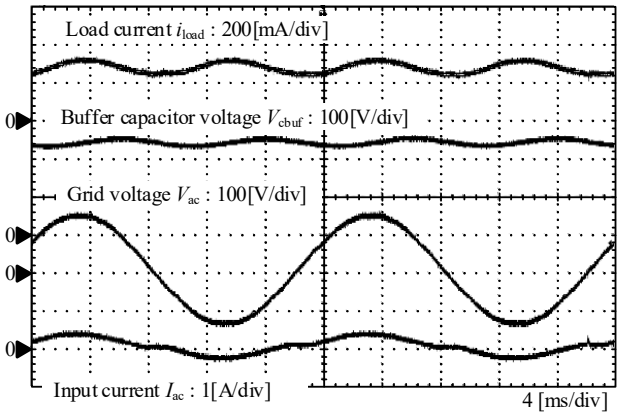

(a) Without proposed control

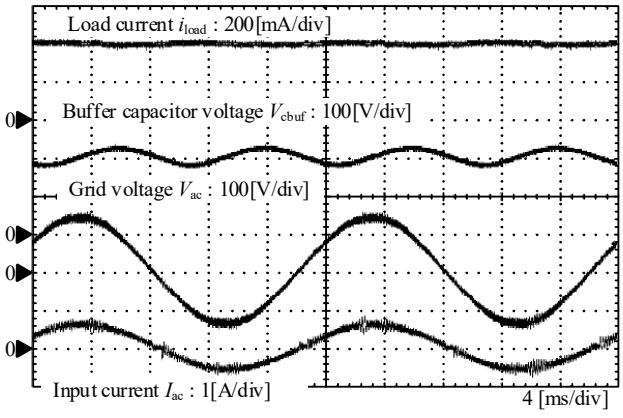

(b) With proposed control

Fig.11 Experimental result.

Power Electronics and Applications (EPE'17 ECCE Europe), pp. 1-9 (2017)

[10] Z. Shan, X. Chen, S. Fan, G. Yuan, C. K. Tse "Resonant Switched-capacitor Auxiliary Circuit for Active Power Decoupling in Electrolytic Capacitor-less AC/DC LED Drivers", *2019 IEEE Energy Conversion Congress and Exposition (ECCE)* ,pp.866-871 (2019)

[11] T. Orgil, B. Dugarjav, T. Shimizu"Active Power-Decoupling Circuit to Reduce Ripple Currents of Recycling Batteries used with Single-Phase Voltage Source Inverters" *IEEE Jour. of Ind. App.*, vol. 10, no.2, pp. 262–263, (2021)

[12] W. Cai; L. Jiang; B. Liu; S. Duan; C. Zou;" A Power Decoupling Method Based on Four-Switch Three-Port DCDCAC Converter in DC Microgrid" *IEEE Trans. Ind. Appl.*, Vol. 51, No. 1, pp. 336-343, (2015)

[13] H. Watanabe, T. Sakuraba, K..Furukawa, K. Kusaka, J. Itoh: "Development of DC to Single-Phase AC Voltage Source Inverter With Active Power Decoupling Based on Flying Capacitor DC/DC Converter", *IEEE Trans. on Power Electron,* Vol. 33, No. 6, pp. (2018)

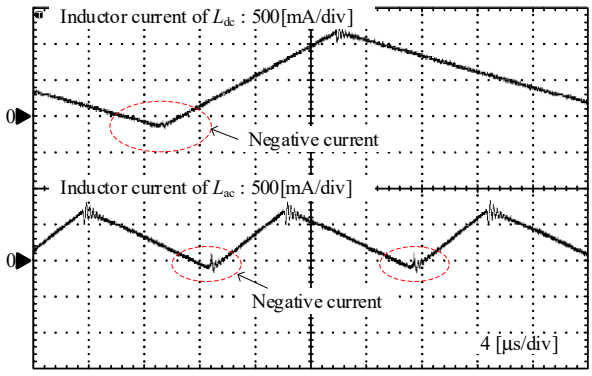

Fig.12 Inductor current waveforms.

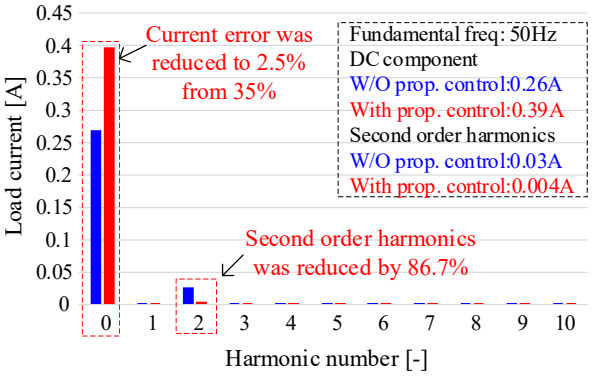

Fig.13 Harmonic analysis result of load current.